Diffusion Maps Segmentation of Magnetic Resonance Q-Ball Imaging

Demian Wassermann[1,2]   Maxime Descoteaux[1]

Rachid Deriche[1]

[1]Odyssée Project Team INRIA/ENPC/ENS

INRIA, Sophia-Antipolis, 2004 Route des Lucioles, 06902 Sophia Antipolis, France

{demian.wassermann,maxime.descoteaux,rachid.deriche}@sophia.inria.fr

[2]Computer Science Department, School of Exact and Natural Sciences, University of Buenos Aires

Pabellón 1, Ciudad Universitaria,C1428EGA Buenos Aires, Argentina

Abstract

We present a Diffusion Maps clustering method applied to diffusion MRI in order to segment complex white matter fiber bundles. It is well-known that diffusion tensor imaging (DTI) is restricted in complex fiber regions with crossings and this is why recent High Angular Resolution Diffusion Imaging (HARDI) such has Q-Ball Imaging (QBI) have been introduced to overcome these limitations. QBI reconstructs the diffusion orientation distribution function (ODF), a spherical function that has its maximum(a) agreeing with the underlying fiber population. In this paper, we use the ODF representation in a small set of spherical harmonic coefficients as input to the Diffusion Maps clustering method. We first show the advantage of using Diffusion Maps clustering over classical methods such as N-Cuts and Laplacian Eigenmaps. In particular, our ODF Diffusion Maps requires a smaller number of hypothesis from the input data, reduces the number of artifacts in the segmentation and automatically exhibits the number of clusters segmenting the Q-Ball image by using an adaptative scale-space parameter. We also show that our ODF Diffusion Maps clustering can reproduce published results using the diffusion tensor (DT) clustering with N-Cuts on simple synthetic images without crossings. On more complex data with crossings, we show that our method succeeds to separate fiber bundles and crossing regions whereas the DT-based methods generate artifacts and exhibit wrong number of clusters. Finally, we show results on a real brain dataset where we successfully segment the fiber bundles.

1. Introduction

Recent work shows that diffusion Magnetic Resonance Imaging (dMRI) can help recovering white matter complex brain architecture. However this is still an open problem due to the structural complexity of the fiber tract bundles, which can have crossing configurations. Diffusion tensor imaging (DTI) [4] is restricted in these conditions due to its hypothesis that the diffusion within a voxel follows a Gaussian distribution, a model that cannot model intra-voxel crossings. Q-ball Imaging (QBI) [28], a recent high angular resolution diffusion imaging (HARDI) technique, overcome this limitation by reconstructing the diffusion orientation distribution function (ODF), a spherical function that has its maxima(um) agreeing with the underlying fiber populations.

The goal of this work is to provide a segmentation method that can recover the white matter brain architecture and that can deal with fiber tract crossings while requiring a minimum number of hypothesis from the data. Spectral embedding and clustering methods have recently proved to be effective in image segmentation [25, 32]. The classical approaches like N-Cuts [25] and Laplacian Eigenmaps [5] require data within each cluster to be uniformly sampled, producing artifacts when this hypothesis is not met. Moreover classical approaches to spectral clustering [25, 24, 5] also assume that the scale within each cluster is the same using a single scale parameter for the whole dataset. In order to overcome these limitations, we use Diffusion Maps [7] as spectral embedding method, which looses the dependence on the sampling of the elements to cluster. Moreover, we use an adaptative scale-space parameter in order to deal with space-scale differences across different clusters. Finally, our approach also allows to automatically determine the number of clusters by analyzing the spectra of the image embedding.

Another contribution of this paper is to show that the Q-ball ODF clustering using Diffusion Maps can reproduce the DT clustering using N-Cuts on simple synthetic images without crossings. On more complex data with crossings, we show that our method succeeds to separate fiber bundles and crossing regions whereas the DT-based methods generate artifacts and exhibit wrong number of clusters. Finally,

1

we successfully segment some important fiber bundles on a real dataset.

2. Methods

The main goal of this work is to produce a segmentation algorithm able to segment dMRI data into fiber bundles and crossings. Although clustering methods in general and the algorithm developed in this work could be applied to the raw signal estimation using a spherical harmonic representation [13, 1, 8], we choose to use the ODF reconstruction as input to our algorithm as it is a very popular object used for fiber clustering, segmentation and tracking. In order to represent intra-voxel crossings with the ODF, we need at least 15 real harmonic coefficients [14, 9]. This leads to 3D images with a high dimensional element at each voxel. This high dimensionality makes previous diffusion imaging segmentation approaches based on Level Set Methods such as [20, 17, 10] computationally expensive. Moreover, these methods require an initialization step. In order to perform the segmentation in an initialization-free manner and with a lower dimensionality image, we use spectral clustering methods [25, 32], which perform dimensionality reduction before performing the segmentation and do not need initialization. The segmentation is then performed on the statistics within each cluster and the fiber crossings can be identified.

In this section, we present the two main parts of our algorithm. First, the estimation of the Q-ball diffusion ODF and its compact representation using spherical harmonics. Second, the Diffusion Maps spectral clustering technique used to segment the ODF image into the background, the different fiber bundles and the crossings areas between these fiber bundles.

2.1. ODF Estimation from QBI

QBI [28] reconstructs the diffusion ODF directly from the N HARDI measurements on a single sphere by the Funk-Radon transform (FRT). The ODF is intuitive because it has its maximum(a) aligned with the underlying population of fiber(s). However, computing statistics on a large number of discrete ODF values on the sphere is computationally heavy and infeasible to integrate into a segmentation algorithm of the whole brain. A more compact representation of the ODF is thus needed. [9, 2, 14] proposed a simple analytical spherical harmonic (SH) reconstruction of the ODF. Letting Y_ℓ^m denote the SH of order ℓ and degree m ($m = -\ell, ..., \ell$) in the standard basis and Y_j ($j(\ell, m) = (\ell^2 + \ell + 2)/2 + m$) be the SH in the modified real and symmetric basis, the final ODF is

$$\Psi(\theta, \phi) = \sum_{j=1}^{L} \underbrace{2\pi P_{\ell(j)}(0) c_j}_{f_j} Y_j(\theta, \phi), \qquad (1)$$

where $0 \le \theta < 2\pi$, $0 \le \phi < \pi$, $L = (\ell + 1)(\ell + 2)/2$, c_j are the SH coefficients describing the input HARDI signal, $P_{\ell(j)}$ is a Legendre polynomial of order $\ell(j)$[1] and f_j the coefficients describing the ODF Ψ. Here, we use the solution presented in [9] with a Laplace-Beltrami regularization of the SH coefficients c_j to obtain a more robust ODF estimation.

Distances between ODFs We want to capture similarities and dissimilarities between two ODFs, i.e two spherical functions $\Psi, \Psi' \in \mathbf{S}^2$. This can be done by taking the Euclidean distance between all N discrete ODF value on the sphere. When the ODFs Ψ, Ψ' are represented by real SH vectors $f, f' \in \mathbb{R}^L$, as shown in the previous section, this Euclidean distance measure can be applied directly on the SH coefficients. Since the ODFs come from real physical diffusion measurements they are bounded and form an open subset of the space of real-valued $\mathcal{L}^2$ spherical functions with an inner product $\langle, \rangle$ defined as

$$
\begin{aligned}
\langle \Psi, \Psi' \rangle &= \int_{\mathbf{S}^2} \Psi(\sigma) \cdot \Psi(\sigma)' d\sigma \\
&= \int_{\mathbf{S}^2} \left(\sum_{i=1}^{L} f_i Y_i(\sigma) \sum_{j=1}^{L} f_j' Y_j(\sigma) \right) d\sigma.
\end{aligned}
\qquad (2)
$$

Because of the orthonormality of the SH basis, $\int_\sigma Y_i(\sigma) Y_j(\sigma) d\sigma = \delta_{ij}$, the cross terms cancel and the expression is simply $\langle \Psi, \Psi' \rangle = \sum_{j=1}^{L} f_j \cdot f_j'$. Therefore, the induced $\mathcal{L}^2$ norm $||\Psi|| = \sqrt{\langle \Psi, \Psi' \rangle}$ giving us the distance metric between two ODFs is simply

$$||\Psi - \Psi'|| = \sqrt{\int_{\mathbf{S}^2} (\Psi(\sigma) - \Psi'(\sigma))^2 d\sigma} = \sqrt{\sum_{j=1}^{L} (f_j - f_j')^2}. \qquad (3)$$

The Euclidean distance was also used successfully for DTI segmentation in [20] even though more appropriate metrics exist such as the J-Divergence [29, 20] and Riemannian geodesic distances [20]. Similarly, one can think of choosing another metric to compare ODFs. For instance, since the ODF can be viewed as a probability distribution function (PDF) of fiber orientations, one can use the Kullback-Leibler distance between two PDFs, as done in [28]. However, in that case the problem quickly blows up computationally because one needs to use all N discrete data on the sphere instead of the L SH coefficients ($L << N$).

2.2. Diffusion Maps

In recent years, spectral manifold learning and clustering techniques[30, 24, 25, 26, 30, 5], have become one of the

---

[1] $\ell(j)$ is the order associated with the jth element of the SH basis, i.e. for $j = 1, 2, 3, 4, 5, 6, 7, ...$ $\ell(j) = 0, 2, 2, 2, 2, 2, 4, ...$

most popular modern clustering family of methods. They are simple to implement, they can be solved efficiently by standard linear algebra software and they very often outperform traditional manifold learning and clustering algorithms such as the classical PCA (Principal Component Analysis) [16] and k-means [15] algorithms. Moreover due to the dimensionality reduction properties they are specially suited to work with high-dimensional data. These techniques have been recently proposed in order, among other things, to cluster various types of images [25, 32] and white matter fiber tracts [23]. In our case we perform the spectral clustering in two different types of elements, the DT and the ODF. In the DT case, the element is represented by a 6-dimensional vector corresponding to each element of the DT 3x3 symmetric matrix. In the ODF case, the element is represented by the 15-dimensional vector corresponding to the spherical harmonic coefficients of the order 4 ODF estimation.

Spectral clustering reduces the clustering problem to a graph partitioning problem. Each element to be clustered is represented as a node in a graph and the edges joining the vertex are a measure of affinity between the elements. This affinity measure lies between 0 and 1, 0 being the less affine case. A spectral decomposition of this graph is taken by calculating the eigenvalue decomposition (EVD) of the graph Laplacian [6]. Then a low-dimensional Euclidean manifold embedding is inferred from this decomposition. Finally, the clustering is performed in the inferred Euclidean manifold.

All the above techniques rely on three hypotheses:

1. Isometry of the embedding: after a distance is defined between elements, the learned manifold should preserve the distance relation.

2. Uniform sampling of the elements: the density of the extracted elements changes if and only if these elements belong to anatomically different bundles.

3. Convexity of the elements: if two elements are in the data set, almost all of the intermediate tracts obtained by interpolation are in the data set.

Its not easy to guarantee that the data to be embedded and clustered will adhere to these hypotheses. In [11], they analyze when a spectral embedding algorithm is able to recover the true parameterization of a set of images. As medical images represent the discretization of a continuous space, hypotheses 1 and 3 are plausible. However there is no indication that within a fiber bundle the distribution of the elements (DT or ODF) are uniformly sampled. Moreover, in [18] it is shown that different sampling frequencies within one cluster leads the N-Cuts and Laplacian Eigenmaps methods to subdivide the cluster in several parts.

In order to overcome this limitation we use the Diffusion Maps [7] spectral embedding technique, which is resilient

to sampling frequency differences within a cluster. In order to further describe the classical spectral clustering and embedding procedure, we first sketch the steps and then describe each step in detail:

Algorithm 1 *For a set X of L-dimensional elements with an affinity function[2] $a : X \times X \to \mathbb{R}_{\geq 0}$, perform the following steps:*

1. *Compute a normalized affinity matrix.*

2. *Perform an embedding $\mathbf{y}(X)$ of X into a n-dimensional Euclidean manifold, $n << L$*

3. *Cluster the elements of X in the embedded space $Y = \mathbf{y}(X)$.*

Step 1: Computing the normalized affinity matrix The main idea of this process is to represent in a more tractable way the relationships between the elements of $f \in X$, $f \in \mathbb{R}^L$, that will be used to cluster them. With this in mind, a fairly good way of representing any set of elements with an affinity function $a : X \times X \to \mathbb{R}_{>0}$, is a weighted graph, $G(X, E, w(\cdot))$ where the weight of the edge between two vertices is equal to the affinity of the elements represented by them. More formally, for an edge[3], $e = (f_i, f_j) \in E$, the weight of the edge is $w(e) = a(f_i, f_j)$. Hence, each element of the adjacency matrix of G or conversely the affinity matrix of $(X, a(\cdot))$ is

$$A_{ij} := a(f_i, f_j),$$

taking this in account, the weighted graph $G(X, E, w(\cdot))$ can be also noted as $G(X, A)$, where $A \in \mathbb{R}^{|X| \times |X|}$.

Nevertheless, the usual set up is a set of elements with a distance function $d(\cdot)$ instead of an affinity function. The distances can be easily converted into affinities by taking a kernel of the distance function:

$$a(f_i, f_j) = e^{-\frac{d(f_i, f_j)^2}{\sigma_{ij}^2}}, \tag{4}$$

where σ is an adaptive scale space parameter that depends on the elements f_i and f_j. The adaptative scale-space parameter is computed as in [31], a "neighbor-number" k is given as parameter to the algorithm and then $\sigma_{ij}^2 = d(f_i, f_{i_k})d(f_j, f_{j_k})$ where f_{i_k} is the k-th closest neighbor according to the distance function $d(\cdot, \cdot)$ of element f_i.

In order to overcome the necessity of hypothesis 2, we pre-normalize the affinity matrix, as done in [7]. This is done by normalizing the weight of each edge of the graph,

---

[2]The function $a(e_i, e_j)$ should be near zero if the two elements are not affine and maximum when $e_i = e_j$.

[3]In this section the subindexed variables f_i, f_j represent different elements to be clustered and not spherical harmonic coefficients.

A_{ij}, by the probability density of both elements relating through the edge,

$$(A_p)_{ij} = \frac{A_{ij}}{p(i)p(j)},$$

where $p(\cdot)$, the probability density function of the elements in X, is not known but can be approximated, up to a multiplication factor, by,

$$p(i) = \sum_k A_{ik} = \sum_k A_{ki}.$$

As in image segmentation, the spatial position of each element is important, the spatial dependency should be incorporated within the affinity matrix. Following [27, 32], we use Markovian Relaxation to incorporate this information. In order to represent the affinity of all the elements that can be reached within 1 spatial step, the affinity matrix is modified in the following way

$$A_{p1_{ij}} = \begin{cases} A_{p_{ij}} & \text{if } \| \operatorname{coords}(f_i) - \operatorname{coords}(f_j)\|_2 \leq r \\ 0 & \text{any other case} \end{cases}$$

where $\operatorname{coords}(f)$ are spatial coordinates of element f in the image and r represents the unit radius circle in the spatial coordinates. Then, to obtain the affinities of elements that can be reached within s spatial steps, it is enough to elevate A_{p1} to the power of s, $A_{ps} = A_{p1}^s$. Moreover, s can be chosen to be the smallest positive integer which gives non-zero elements in the whole matrix in order to represent the weakest connected induced graph.

Due to the necessity of having a uniform behavior of the clustering algorithm without minding the scale of the affinity measure taken, a doubly stochastic matrix normalization is performed

$$\tilde{A_{ps_{ds}}} := D(A_{ps})^{-1/2} A_{ps} D(A_{ps})^{-1/2} \in \mathbb{R}^{|X| \times |X|},$$

where $D(A_{ps})$ is the row-sum matrix or degree matrix of A_{ps}. In the following sections we will address the normalized affinity matrix $\tilde{A_{ps_{ds}}}$ as A for the sake of clarity.

Step 2: Performing the embedding Now the algorithm must perform an embedding of the elements in X into an n-dimensional Euclidean space, by using the eigenvalue decomposition of the Laplacian of the affinity matrix. This embedding must be compliant with hypothesis 1. More formally the algorithm should find mapping function $\mathbf{y} : X \to R^n$, $n \ll L$. This problem can be formulated as finding a mapping that minimizes the following energy

$$\sum_{i,j=1}^{|X|} (\mathbf{y}_i - \mathbf{y}_j)^2 A_{ij}, \mathbf{y}_i, \mathbf{y}_j \in \mathbb{R}^n, \tag{5}$$

where $\mathbf{y}_i = \mathbf{y}(f_i)$, $f_i \in X$. As in [7, 6, 5], this is equivalent to find the spectral decomposition of the graph Laplacian of the graph induced by A,

$$\Delta = D(A) - A \in \mathbb{R}^{|X| \times |X|},$$

where $|X|$ is number of elements to be clustered, however, as A is a double stochastic matrix, this equation can be rewritten as

$$\Delta = I - A \in \mathbb{R}^{|X| \times |X|},$$

then, as A is a symmetric positive definite matrix, the eigenvalue decomposition can be calculated by taking the Singular Value Decomposition (SVD),

$$V S V^T = A \in \mathbb{R}^{|X| \times |X|},$$

where,

$$V = \left(\mathbf{v}^0 \cdots \mathbf{v}^{|X|-1} \right) \in \mathbb{R}^{|X| \times |X|}$$

is the eigenvector column matrix and S is a diagonal matrix with the sorted eigenvalues in the diagonal, $1 = \lambda_0 \geq \lambda_1 \geq \cdots \geq \lambda_{|X|-1} \geq 0$.

Finally the Euclidean coordinates $\mathbf{y}_i$ of an element $f_i \in X$ in the n-dimensional embedding manifold, $n < min(L, |X|)$ are

$$\mathbf{y}(f_i) = \mathbf{y}_i = \frac{1}{\mathbf{v}_i^0} \left(\lambda_1 \mathbf{v}_i^1, \ldots, \lambda_n \mathbf{v}_i^n \right)^T , f_i \in X$$

where the first eigenvalue, λ_0, is not taken into account because it is constant and hence meaningless, as shown in [7, 6, 5].

Step 3: Clustering Once the embedding has been performed, several techniques have been proposed for the clustering step.

The first step in this process is to determine the number of clusters, this can be done in two ways. The first, as in [22], is choosing the number of clusters according to the "elbow" than can be devised in the eigenvalues plot. For instance, if the slope of the eigenvalues plot changes noticeably at eigenvector λ_i, the number of clusters should be $i+1$. The second way is re-ordering the affinity matrix rows and columns following the second eigenvector, as proved in [12], which shows the block structure of the matrix as squared blocks along the matrix diagonal. Then, the number of clusters is the number of blocks. The recommended number of dimensions for the embedding is the same as the number of clusters. Finally, the clustering is performed by running a k-means clustering algorithm on this space. A formal justification for this approach can be found in [5, 19].

2.3. Q-Ball Data Generation and Acquisitions

Synthetic Data We generate synthetic Q-ball data using the multi-tensor model [28], $S(\mathbf{u}_i) = \sum_{k=1}^{n} \frac{1}{n} \exp(-b\mathbf{u}_i^{\mathrm{T}}\mathbf{D_k}(\theta)\mathbf{u}_i) + noise$, for N encoding directions $i \in \{1, ..., N\}$. We use $N = 81$ from a 3rd order tessellation of the icosahedron, $b = 3000$ s/mm^2, $n = 1$ or 2 and $\mathbf{D_k}(\theta)$ the diffusion tensor with standard eigenvalues $[3, 3, 1.7]$x10^{-2} mm^2/s oriented in direction θ [28, 9]. The noise is generated with a complex Gaussian noise with a standard deviation of $1/35$, producing a signal with SNR 35. We generate three synthetic data example, two simple examples, one with a ring of sinusoidal shaped fibers, one with fibers with different sizes and scales and the other with complex crossing areas simulating the 'U'-fibers (cortico-cortical fibers) that can occur in the brain. These synthetic datasets help understand the behavior of the different spectral clustering methods when confronted with simple and complex fiber geometries.

Human Brain Data We use a human brain dataset acquired on 3T scanner [3] with 60 encoding directions, $b = 1000$ s/mm^2, 72 slices with 1.7mm thickness, twenty one $b = 0$ s/mm^2 images, 128 x 128 image matrix, TE $= 100$ ms, TR $= 12$ s.

Distance functions In order to implement the Diffusion Maps spectral clustering method a distance function for each data type is chosen. This distance functions are used in order to calculate the affinity matrix as expressed by equation (4). In the DT case, following [21], we use the Riemannian tensor distance. In the ODF case we use the distance shown in equation (3).

3. Results and Discussion

3.1. Synthetic data experiments

Diffusion Maps vs. N-Cuts The first experiment shows the difference in performance between the Diffusion Maps and N-Cuts approach. In order to do this we used the ring fiber bundle image. This fiber bundle has different sampling frequencies. Within the ring, the fibers have a sinusoidal shape where the frequency of the modulating sine function is 4 times bigger in the lower half of the ring. More formally, the fibers follow the angular function $o(\theta) = \theta + \frac{1}{8}\pi \sin(\mu \cdot \theta), 0 \leq \theta < 2\pi$, where $\mu = 8$ for the upper half of the ring and $\mu = 32$ for the lower half. Two clusters are expected, the ring and the background. The results of both clustering techniques are shown in figure 1, where the background has been masked out. Following the plot of the biggest 10 eigenvalues for both methods, shown in figure 1(f) and figure 1(e), the number of clusters to be chosen should be either 2 or 4. The N-Cuts exhibits

frequency-dependent clustering artifacts in both cases, figure 1(a) and 1(c), while the Diffusion Maps method clearly shows the expected result with two clusters shown in figure 1(d).

ODF vs. DT images The second experiment shows a simple fiber tract scenario (figure 2), which does not include fiber crossings. The DT-based and ODF-based image clustering produce the same results.

Finally, the last synthetic experiment is performed over the fiber crossing scenario presented in figure 3. The two overlapping fiber bundles have different geometries. Segmentation was performed over the DT and the ODF image shown in figure 4. Note that the cluster number is correctly estimated only in the ODF image. The ODF Diffusion Maps effectively identify the two different fiber bundles as well as the fiber crossing areas.

3.2. Real Data

The real data experiment presented in this section shows the segmentation and labeling of a cropped axial and coronal slice. The cropped slices were chosen by an expert in regions of known fiber crossings where the DT model is normally limited. The ROIs show intersection of several fiber bundles. Hence, our segmentation algorithm is confronted with elements that have different orientation and different diffusion characteristics. In order to show that ODF data segments the white matter fiber bundles better than the DT data in real cases, we analyze the evolution of the affinity matrix as the scale space parameter changes in the axial cropped slice shown in figure 5. Affinity matrices were computed with varying scale space parameter between $\frac{1}{5}$, $\frac{1}{10}$, $\frac{1}{20}$ and $\frac{1}{40}$ of the quantity of elements ($|X|$) to cluster respectively. In order to show the block structure of the affinity matrices, they were reordered using the second (Fiedler) biggest eigenvector [12]. It can be seen in figure 6 that as the scale diminishes, the DT data shows a high correlation between all the elements of the slice. This makes clustering very difficult because the blocks are small and highly correlated. On the other hand, the ODF data shows a very clear block structure across all scales. This block structure shows a high correlation of the elements within each block and a low inter-block correlation, giving a much better input to the clustering algorithm than the DT data.

In figure 5, the location of the cropped axial slice is shown in the axial slice and coronal slices. As it can be seen in the segmented and labeled axial slice, figure 7, the segmentation also allows to identify and label the main white matter structures, Corpus Callosum (CC), Cingulum (CG) and the Corona Radiata (CR).

In figure 8, the location of the cropped coronal slice is shown in the axial slice and coronal slices. As it can
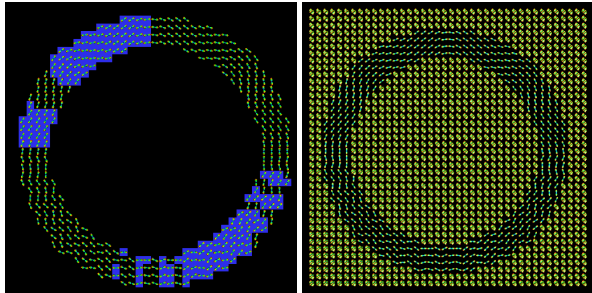
(a) N-Cuts, 2 clusters (blue and (b) Original ODF image
black)
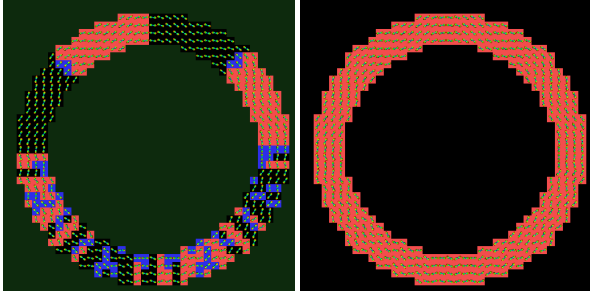
(c) N-Cuts, 4 clusters (blue, red, (d) Diffusion Maps, 2 clusters
green and black) (red and black)
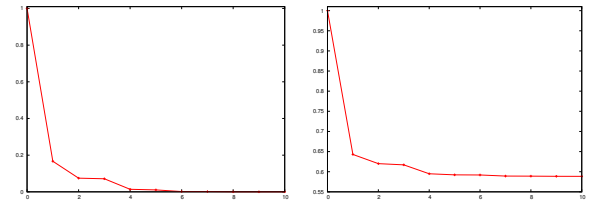
(e) N-Cuts eigenvalue plot (f) Diffusion Maps eigenvalue
plot

Figure 1. N-Cuts generates over-clustering due to sampling frequency variation in ODF images. The original image 1(b) without ommiting the background. Between 2 and 4 clusters are found and the clustering results with 2, 1(a), and 4, 1(c), clusters are shown. Diffusion Maps correctly finds two clusters, the object and the background, 1(d) .. In the labeling, the ODFs are overlaid on the labels, in the clustering images the background is omitted for clarity.

be seen in the segmented and labeled coronal slice, figure 3.2, the segmentation allows to identify and label the main white matter structures: Corpus Callosum (CC), Cingulum (CG), Corona Radiata (CR), Superior Longitudinal Fasciculus (SLF). Note that the segmentation is resilient to crossing areas such as seen at the interface between CR and CC.
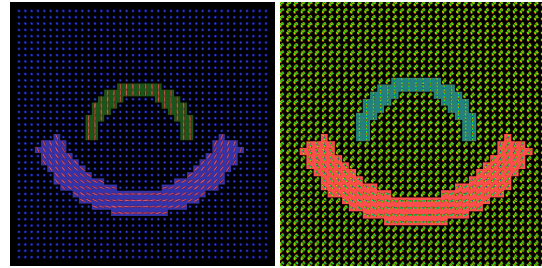
(a) DTI (b) ODF

Figure 2. Synthetic image. On fiber tracts without crossings the results over DT and ODF images are equivalent. The colors behind the DTs and ODFs indicate the cluster.
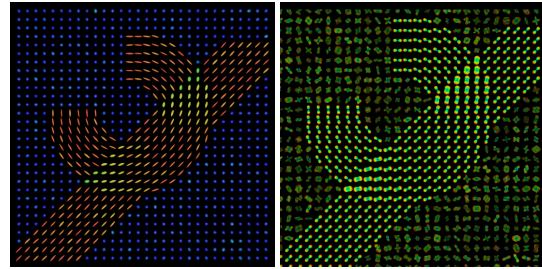
(a) DTI (b) ODF

Figure 3. Synthetic image. The expected number is four, one for each fiber, one for the crossing between the two fibers and one for the background
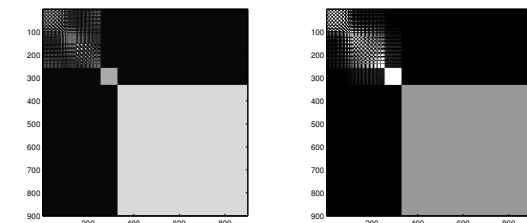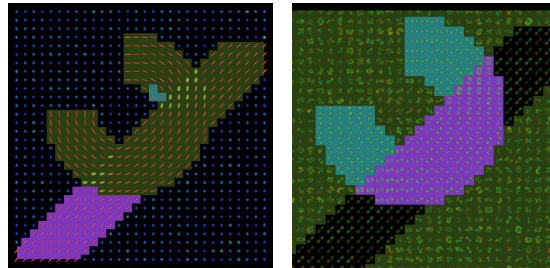
(a) DTI (b) ODF

Figure 4. Clustering results in ODF and DT images, Only ODF show the correct clustering. In both cases the clustering result and the reordered affinity matrix are shown.

4. Conclusions

In this work, we have presented two contributions. First, we have shown that in order to perform spectral clustering
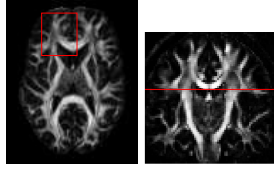
Figure 5. Generalized fractional anisotropy axial and coronal slices in the real dataset with the axial region marked

(a)   DTI reordered affinity matrices

(b)   ODF reordered affinity matrices
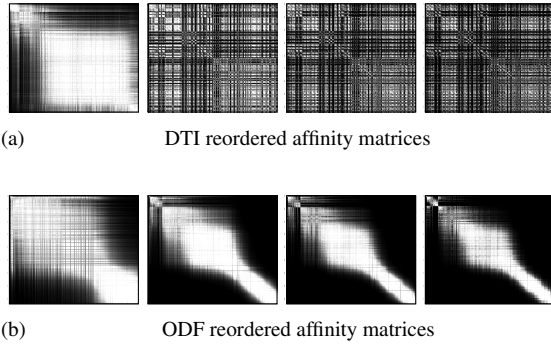
Figure 6. Plots of DTI and ODF affinity matrices of an axial cropped slice shown in figure 5. The matrices are reordered according to the second (Fiedler) eigenvector. The affinity matrices are shown in decreasing order of σ, which takes the values $\frac{1}{5}$, $\frac{1}{10}$, $\frac{1}{20}$ and $\frac{1}{40}$ of the quantity of elements to cluster.
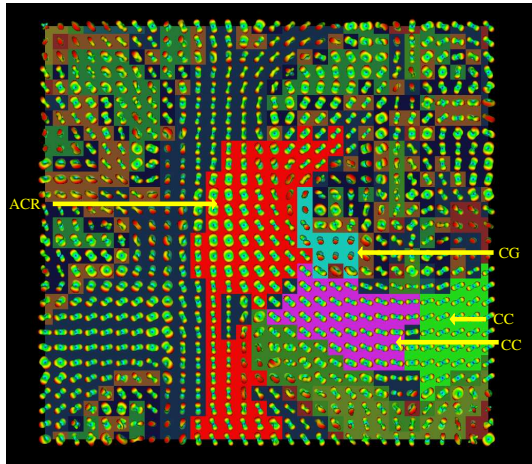
Figure 7. Our proposed algorithm is able to identify important white matter fiber bundles on an axial slice of a real dataset. The cropped axial slice shown in figure 3.2 has been segmented. In the labeled ODF visualization, each color represents one of the clusters found. The white matter labels are CC: Corpus Callosum, CG: Cingulum, ACR: Anterior Corona Radiata.

on complex dMRI with crossing fiber bundles, a HARDI technique such as Q-Ball Imaging is better than the classical DTI technique. This is because the ODF reconstructed from QBI is able to recover multiple crossing fiber populations.
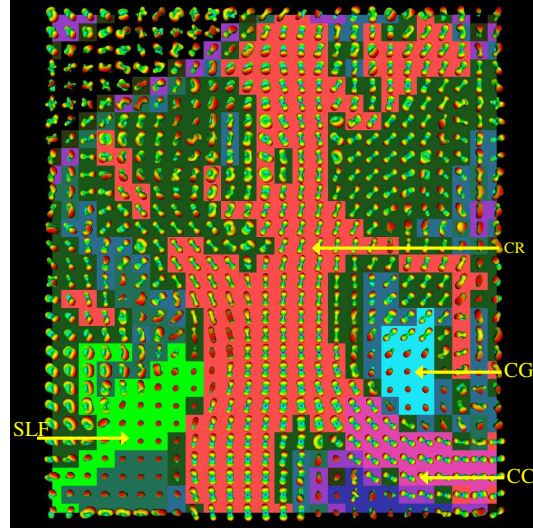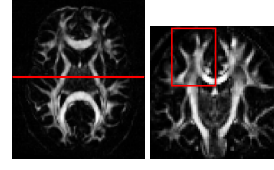
Figure 8. Our proposed algorithm is able to identify important white matter fiber bundles on a coronal slice of a real dataset. Generalized fractional anisotropy axial and coronal slices are shown with the coronal region marked. Labeled ODF visualization, each color represents one of the 12 clusters found. The white matter labels are CC: Corpus Callosum, CG: Cingulum, CR: Corona Radiata, SLF: Superior Longitudinal Fasciculus.

Secondly, a Diffusion Maps based technique for image segmentation was introduced to improve the segmentations and to reduce artifacts arising from the widely used N-Cuts image segmentation. We have illustrated the consequences of the theoretical advantages of the Diffusion Maps ODF segmentation algorithm, and shown in a real data set that our algorithm is able to identify the most important white matter complex structures.

Finally, the Diffusion Maps technique has been shown to be more robust to sampling frequency variations within each object to segment. This is shown in section 3.1 and illustrated in figure 1. In order to cluster the elements in the space spanned only by the tensors we have used an adaptative scale-space parameter and we have used Markovian Relaxation in order to incorporate spatial dependencies. Overall, the approach is theoretically sound with the graph based representation which lies at the heart of spectral clustering methods.

References

[1] D. C. Alexander, G. J. Barker, and S. R. Arridge. Detection and modeling of non-gaussian apparent diffusion coefficient profiles in human brain data. *Magn Reson Med*, 48(2):331–340, Aug 2002.

[2] A. Anderson. Measurements of fiber orientation distributions using high angular resolution diffusion imaging. *Magnetic Resonance in Medicine*, 54:1194–1206, 2005.

[3] A. Anwander, M. Tittgemeyer, D. Y. von Cramon, A. D. Friederici, and T. R. Knosche. Connectivity-based parcellation of broca's area. *Cerebral Cortex*, 17(4):816–825, 2007.

[4] P. Basser and D. Jones. Diffusion-tensor MRI: theory, experimental design and data analysis- a technical review. *NMR in Biomedicine*, 15(7-8):456–467, 2002.

[5] M. Belkin and P. Niyogi. Laplacian eigenmaps for dimensionality reduction and data representation. *Neural Computation*, 15(6):1373–1396, jun 2003.

[6] F. Chung. *Spectral graph theory*. CBMS-AMS, 1997.

[7] R. Coifman, S. Lafon, A. Lee, M. Maggioni, B. Nadler, F. Warner, and S. Zucker. Geometric diffusions as a tool for harmonic analysis and structure definition of data: Diffusion maps. *Proceedings of the National Academy of Sciences*, 102(21):7426–7431, may 2005.

[8] M. Descoteaux, E. Angelino, S. Fitzgibbons, and R. Deriche. Apparent diffusion coefficients from high angular resolution diffusion images: Estimation and applications. *Magnetic Resonance in Medicine*, 56(2):395–410, aug 2006.

[9] M. Descoteaux, E. Angelino, S. Fitzgibbons, and R.Deriche. A fast and robust odf estimation algorithm in q-ball imaging. In *Third IEEE International Symposium on Biomedical Imaging: from Nano to Macro*, pages 81–84, Arlington, Virginia, USA, Apr. 2006.

[10] M. Descoteaux and R. Deriche. Segmentation of q-ball images using statistical surface evolution. In Springer, editor, *Medical Image Computing and Computer-Assisted Intervention (MICCAI)*, volume LNCS, page to appear, Brisbane, Australia, 2007.

[11] D. L. Donoho and C. Grimes. Image manifolds which are isometric to euclidean space. *Journal of Mathematical Imaging and Vision*, 23:5–24, 2005.

[12] M. Fiedler. A property of eigenvectors of nonnegative symmetric matrices and its application to graph theory. *Czechoslovak Mathematical Journal*, 25:619–633, 1975.

[13] L. R. Frank. Characterization of anisotropy in high angular resolution diffusion-weighted mri. *Magn Reson Med*, 47(6):1083–1099, Jun 2002.

[14] C. Hess, P. Mukherjee, E. Han, D. Xu, and D. Vigneron. Q-ball reconstruction of multimodal fiber orientations using the spherical harmonic basis. *Magnetic Resonance in Medicine*, 56:104–117, 2006.

[15] A. Jain, M. Murty, and P. Flynn. Data clustering: a review. *ACM Computing Surveys (CSUR)*, 31(3):264–323, 1999.

[16] I. Jolliffe. *Principal component analysis*. Springer Series in Statistics, Berlin, 1986.

[17] L. Jonasson, P. Hagmann, C. Pollo, X. Bresson, C. Wilson, R. Meuli, and J. Thiran. A level set method for segmentation of the thalamus and its nuclei in DT-MRI. *Signal Processing*, 87:309–321, 2007. Special Issue of Signal Processing on Diffuision Tensor Imaging.

[18] S. Lafon. *Diffusion Maps and Geometric Harmonics*. PhD thesis, Yale University, 2004.

[19] S. Lafon and A. Lee. Diffusion maps and coarse-graining: a unified framework for dimensionality reduction, graph partitioning, and data set parameterization. *Pattern Analysis and Machine Intelligence, IEEE Transactions on*, 28(9):1393–1403, Sep 2006.

[20] C. Lenglet, M. Rousson, and R. Deriche. DTI segmentation by statistical surface evolution. *Medical Imaging, IEEE Transactions on*, 25(6):685–700, June 2006.

[21] C. Lenglet, M. Rousson, R. Deriche, and O. Faugueras. Statistics on the manifold of multivariate normal distributions: Theory and application to diffusion tensor mri processing. *J Math Imaging Vis*, 25:423–444, 2006.

[22] B. Nadler, S. Lafon, R. R. Coifman, and I. G. Kevrekidis. Diffusion maps, spectral clustering and eigenfunctions of Fokker-Planck operators. In Y. Weiss, B. Schölkopf, and J. Platt, editors, *Advances in Neural Information Processing Systems 18*, pages 955–962. MIT Press, Cambridge, MA, 2006.

[23] L. O'Donnell and C.-F. Westin. High-dimensional white matter atlas generation and group analysis. In R. Larsen, M. Nielsen, and J. Sporring, editors, *MICCAI*, volume 4191 of *Lecture Notes in Computer Science*, pages 243–251. Springer, 2006.

[24] S. T. Roweis and L. K. Saul. Nonlinear Dimensionality Reduction by Locally Linear Embedding. *Science*, 290(5500):2323–2326, 2000.

[25] J. Shi and J. Malik. Normalized cuts and image segmentation. *Pattern Analysis and Machine Intelligence, IEEE Transactions on*, 22(8):888–905, Aug. 2000.

[26] J. Tenenbaum, V. Silva, and J. Langford. A Global Geometric Framework for Nonlinear Dimensionality Reduction. *Science*, 290(5500):2319, 2000.

[27] N. Tishby and N. Slonim. Data clustering by markovian relaxation and the information bottleneck method. In *Neural Information Processing Systems*, 2000.

[28] D. Tuch. Q-ball imaging. *Magnetic Resonance in Medicine*, 52(6):1358–1372, 2004.

[29] Z. Wang and B. C. Vemuri. Dti segmentation using an information theoretic tensor dissimilarity measure. *IEEE Transactions in Medical Imaging*, 24(10):1267–1277, 2005.

[30] Y. Weiss. Segmentation using eigenvectors: a unifying view. In *International Conference on Computer Vision*, volume 2, pages 975–982, 1999.

[31] L. Zelnik-Manor and P. Perona. Self-tuning spectral clustering. *Advances in Neural Information Processing Systems*, 17:1601–1608, 2004.

[32] U. Ziyan, D. Tuch, and C.-F. Westin. Segmentation of thalamic nuclei from dti using spectral clustering. In *Medical Image Computing and Computer-Assisted Intervention*, Lecture Notes in Computer Science, pages 807–814. Springer/Verlag, 2006.